Molecular, Supramolecular, and Macromolecular Motors and Artificial Muscles

Dongbo Li, Walter F. Paxton,
Ray H. Baughman, Tony Jun Huang,
J. Fraser Stoddart, and Paul S. Weiss

Abstract

Recent developments in chemical synthesis, nanoscale assembly, and molecular-scale measurements enable the extension of the concept of macroscopic machines to the molecular and supramolecular levels. Molecular machines are capable of performing mechanical movements in response to external stimuli. They offer the potential to couple electrical or other forms of energy to mechanical action at the nano- and molecular scales. Working hierarchically and in concert, they can form actuators referred to as artificial muscles, in analogy to biological systems. We describe the principles behind driven motion and assembly at the molecular scale and recent advances in the field of molecular-level electromechanical machines, molecular motors, and artificial muscles. We discuss the challenges and successes in making these assemblies work cooperatively to function at larger scales.

Introduction

The rapid scaling of electronic devices and other structures to smaller dimensions has driven intense study of new techniques for the assembly and construction of devices and machines with functional components based on nanometer-scale building blocks. In the last few decades, remarkable advances in chemical synthesis, nanoscale assembly, and molecular measurements have enabled the development of such molecular-scale machines. A variety of nanoscopic species, including single molecules,[1–3] supramolecular assemblies (a discrete number of molecules connected through noncovalent bonds),[4–6] nanoparticles,[7,8] nanowires,[9–11] and nanotubes,[12–16] have been used as components, each offering unique mechanical properties. Ultimately, success at miniaturization will extend the macroscopic concept of machines to the molecular level.

In principle, a molecular machine consists of a discrete number of molecules or other nanoscale components, each capable of performing mechanical movements in response to external stimuli.[17] While such machines can be as simple as single molecules undergoing conformational changes, they also may function hierarchically and in concert, performing complex functions in analogy to biological systems. One of the most promising examples of this complexity to date, artificial muscle, is discussed in this overview article.

Like their macroscopic counterparts, molecular machines must be powered by electrical,[1,3] chemical,[18] electrochemical,[19] or optical[20–23] means. Although certain key examples of such mechanical coupling are already understood, new strategies for energetic coupling at the nanoscale will enable new applications. Thus, understanding the stimulus-response behavior of molecules and assemblies at the nanometer scale is critical for the practical implementation and optimization of molecular machines.

We survey recent progress toward the control and understanding of nanomechanical motion in prototypical molecular systems. Although there are a variety of artificial molecular machines, such as molecular logic gates[24] and molecular tweezers of DNA[25], we focus primarily on three classes of artificial molecular machines that have proven especially promising in this rapidly developing field: electric field–driven single-molecule switches, chemically or electrochemically actuated bistable rotaxane molecular motors, and electrochemically powered carbon nanotube-based artificial muscles. In each area, we discuss the fundamental principles of molecular assembly, nanomechanical performance characteristics of the single- or supramolecular species, and the physical mechanism underlying stimulated molecular motion. We also analyze the technological challenges and perspectives associated with improving the performance of each molecular machine.

Electric Field–Driven Single-Molecule Conductance Switching

Attempts to miniaturize microelectronic devices to the nanometer scale have led to tremendous research efforts to exploit synthetic and biological molecules as active components of devices. In order to gain insight into how molecules and assemblies function as self-contained nanoelectronic and nanomechanical devices, understanding the behavior of individual molecules and supramolecular assemblies is of critical importance.[3,26–28] The key challenges for this research include not only fabricating precise assemblies of molecules in controlled environments but also accessing their properties and functions at the molecular and nanometer scales. Recently, self- and directed assembly (methods to organize molecules and to control their placement based on chemical and noncovalent interactions for self-assembly; also, processing conditions and processing order for directed assembly) in combination with scanning probe microscopy techniques have led to significant progress in electric field–driven single-molecule switching. Here, we discuss detailed experimental observations of the switching of individual and bundled molecules and the mechanism behind driven motion.

Current challenges and future perspectives on utilizing single molecules as switches and developing them into nanometer electromechanical devices are summarized.

Self-Assembly and Measurements

In order to study and to control the environment and thus the stability of single-molecule switches and motors, these molecules are inserted into two-dimensional self-assembled monolayer (SAM) matrices.[3,26,27,29–31] Alkanethiolate molecules ($C_nH_{2n+1}S^-$) in the matrix have low electrical conductivity and low chemical reactivity, and when assembled into monolayers, their dynamics are understood sufficiently to allow straightforward control and manipulation. In addition, specific types of interactions can be designed and positioned into the functional molecules and their surrounding matrices.[3,27,32,33] All of these favorable features make alkanethiolate monolayers well suited for serving as host matrices for insertion of target molecules.[34–36] Figure 1a schematically shows the process of inserting guest molecules into an n-alkanethiolate SAM on Au{111}, which serves as the substrate surface for the formation of SAM, the physical support and connection, and one of the electronic contacts. Figure 1b shows a molecular-resolution scanning tunneling microscopy (STM) image of a typical alkanethiolate SAM, in which a number of different types of defects, including domain boundaries, step edges, gold substrate vacancy islands, and disordered SAM regions, are observed.[3] These defects and their densities can be controlled by processing the matrix.[37,38] After exposing the alkanethiolate SAMs to guest molecules either in solution, vapor, or by contact (e.g., with a patterned polymer stamp), single molecules can be selectively inserted at the defect sites.[3,23,26,27,30,31,39–45] Due to physical constraints from the surrounding matrix and (optional) designed intermolecular interactions, the inserted molecules are limited in their motion and stabilized in specific conformations. The resulting surface structure, as shown in Figure 1c, consists of isolated molecules protruding from host SAM matrices, enabling measurements of driven molecular switching at the single-molecule level by STM.[39]

In this measurement configuration, a sharp metallic STM tip addresses the isolated molecule and creates a circuit with the molecule and substrate, in which the tip serves as top electrode and the gold substrate as the bottom electrode.[31,39,46,47] Although STM images convolve the probe tip and surface structures and therefore
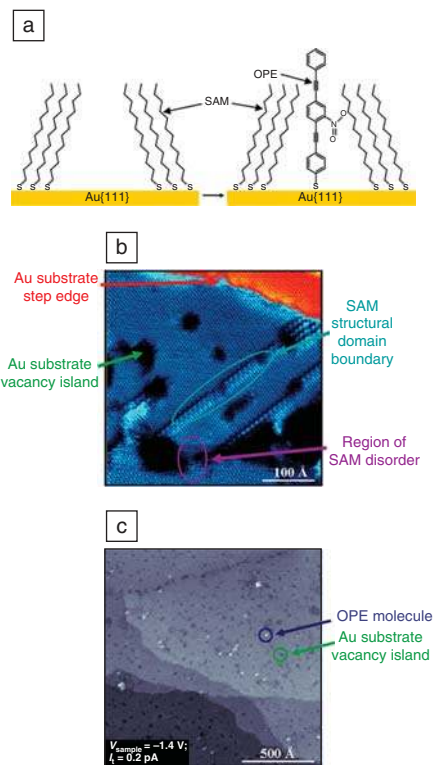
Figure 1. (a) Schematics of an alkanethiolate self-assembled monolayer (SAM) formed by solution deposition (left) and a nitro-functionalized oligo(phenylene ethynylene) (OPE) molecule (4-(2'-nitro-4'-phenylethynyl-phenylethynyl)-benzenethiol (NPPB) inserted into a defect site in the host SAM (right). (b) Molecular-resolution scanning tunneling microscopy (STM) image of a decanethiolate SAM on Au{111} with different types of defects into which single molecules or bundles of other molecules can be inserted. Image courtesy of T.J. Mullen. Reprinted with permission from Reference 3. ©2008, American Chemical Society. (c) STM image (1500 Å × 1500 Å) of OPE molecules inserted into defect sites on an alkanethiol SAM. The vertical scale is ~30 Å. OPE molecules appear as protrusions when oriented near normal to the surface. V_{sample}, sample bias; I_t, tunneling current. Reprinted with permission from Reference 39. ©2001, American Association for the Advancement of Science.

have limited abilities to distinguish single functional molecules from bundles,[40] the specific defect type typically determines whether one versus several molecules have been inserted at a particular site.[31,39,40] Assembly conditions can be selected to favor one or the other, and data can be analyzed to record essentially

exclusively single functional molecules,[39] pairs,[48] or larger bundles.[3]

Single-Molecule Switching

Molecular and supramolecular electronic devices benefit from rational design of the component molecular structure; strategic placement of functionality can give a high level of control over the interactions between molecular electronic devices and their environment.[41–43,49–51] Highly conjugated molecules, such as oligo(phenylene ethynylene)s (OPEs), polyporphyrins, polythiophenes, and polyphenylenes, have been targeted for such devices due to their relatively high electrical conductivity.[32,33,35,42,52,53] Isolating single molecules of OPE derivatives within defect sites of n-alkanethiolate SAMs[38,39,51,54] is a convenient way to study single, isolated molecules over long timescales (hours and longer). Using the electric field between the STM probe tip and the substrate, OPE derivatives with sufficiently large dipole moments can be driven between two states: a high conductance "on" state, in which molecules appear as protrusions of several Ångstroms from the host matrix SAM, and a low conductance "off" state, with molecules either slightly protruding from or at the same apparent height as the matrix in STM images (Figure 2).[39,55,56] Since OPE molecules are more conductive and longer than the dodecanethiolate molecules of the host SAM, they appear as protrusions in STM images (Figure 2a) when oriented near normal to the surface.

Such switching also occurs stochastically, but this stochastic motion can be reduced or eliminated by stabilizing one or both states of the functional molecules by building intermolecular interactions into the functional molecules and the surrounding matrix.[3,43,51,55]

Control of Molecular Switching

Chemical functionality and molecular design of both inserted molecular electronic components and their host SAMs play critical roles in switching.[43,51] Using an alkanethiolate SAM matrix with buried amide functionality, such as 3-mercapto-N-nonyl-propionamide (1ATC9), provides a sizeable increase in the rigidity of the host matrix due to hydrogen bonding between molecular chains and vastly decreases the stochastic switching rate of embedded molecules.[43] Functionality of the inserted molecule also can have a large effect on switching activity; the interaction of the applied electric field with the molecular dipole drives switching.[51] Introduction and modification of the OPE permanent dipole has been accomplished by amination, nitration, and halogenation. By selective

functionalization, both the dipole magnitude and direction can be selected. Figure 3 schematically shows interactions between molecular dipoles and biased STM probes.[51] As shown in the figure, two OPE analogues with opposite dipole directions—a nitro-functionalized OPE molecule (Figure 3a) and an amine-functionalized, pentafluorinated OPE molecule (Figure 3b)—were inserted into SAM matrices with buried functionality tailored to stabilize their different conformations. When a negative tip bias was applied to the nitro-functionalized OPE, the electrostatic attraction drove the molecule to its high-conductance "on" state, a conformation nominally normal to the surface. Conversely, the opposite bias polarity drove the molecule into its low-conductance, or "off" state, with a conformation tilted from the normal. In contrast, the amino-pentafluorinated OPE, with its reversed dipole relative to the nitro-functionalized OPE, was driven into its "on" state with a positive tip bias and its "off" state with a negative tip bias. Importantly, this molecular switching is reversible and can be driven by the electric field applied by the STM tip. Bundles of molecules in crystalline domains switched together; adjacent domains could be switched independently.[3,39] This phenomenon may enable coordinated motions in properly assembled systems. We note that for equivalent photoisomerized one- and two-dimensional clusters of azobenzene-functionalized molecules, switching efficiency is reduced substantially by steric effects and electronic coupling of proximate molecules that ultimately switch together.[23] Such effects will be exploited to produce artificial muscles at the smallest scales.

Recent advances[3,43,51] have enabled the design, assembly, and characterization of single-molecule switches based on isolating functional molecules in matrices. The switching mechanism involves the conformational changes of molecules driven by the applied electric field interacting with the dipoles of the molecules. Host matrices can be used to isolate molecules for single-molecule studies and also play important roles in stabilizing the molecular states. We anticipate that designing and realizing such precise supramolecular interactions will be one of the essential parameters in controlling the overall behavior of assembled molecular devices.

Rotaxane-Based Redox-Driven Molecular Machines

Another important class of artificial single-molecule machines is based on mechanically interlocked molecular
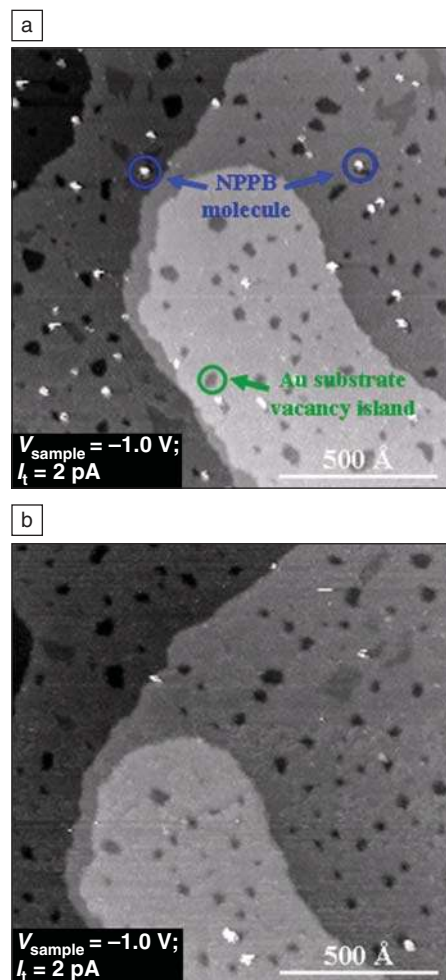

Figure 2. Driven switching is observed in scanning tunneling microscopy (STM) images (1400 Å × 1400 Å) for 4-(2'-nitro-4'-phenylethynyl-phenylethynyl)-benzenethiol (NPPB) molecules inserted into host amide-containing alkanethiol self-assembled monolayer matrices composed of 3-mercapto-N-nonyl-propionamide (1ATC9). (a) The NPPB molecules are in the high conductance "on" state and appear as protrusions; (b) the molecules have been switched to the low conductance "off" state after scanning at the appropriate bias. Reprinted with permission from Reference 43. ©2004, American Chemical Society.

systems (MIMS), highlighted here for their potential use as artificial molecular muscles. These truly molecular systems—comprised of components linked not by covalent bonds but rather by mechanical ones—exhibit an unusual property in that the individual interlocked components can move relative to one another, yet remain part of the molecule.
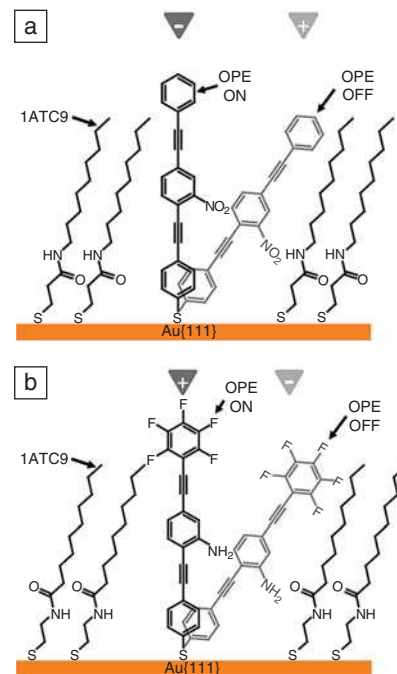

Figure 3. Schematics of interactions between the molecular dipole and the local electric field from a scanning tunneling microscope tip. (a) The nitro-functionalized oligo(phenylene ethynylene) (OPE) molecule 4-(2'-nitro-4'-phenylethynyl-phenylethynyl)-benzenethiol (NPPB) is inserted into a matrix of 3-mercapto-N-nonyl-propionamide (1ATC9). A negative tip bias draws the molecule to the near normal "on" state; the molecule tilts to the "off" state with a positive tip bias. (b) The dipole for the amine-functionalized pentafluorinated molecule shown is inverted compared to NPPB; the amide group orientation in the matrix has been reversed relative to the 1ATC9 matrix used for NPPB. Because of the inverted dipole, the opposite behavior from NPPB is observed. Reprinted with permission from Reference 51. ©2005, American Chemical Society.

Most MIMs can be categorized as either catenanes, in which two or more molecular rings (macrocycles) are mechanically interlocked as in a chain, or rotaxanes, where one or more macrocycles are trapped on a linear rod terminated by bulky groups (stoppers) attached to each end of the rod. The bottom-up assembly of these MIMS is based on templation,[57–59] making use of intermolecular [π-π] and hydrogen bonding interactions to bring individual components together. The relative motion of the interlocked components can be controlled by introducing complementary "stations," where the compo-

nents of the mechanically interlocked compounds recognize each other through relatively weak noncovalent interactions. Furthermore, carefully designed compounds can incorporate recognition stations that can be turned "on" or "off" by a variety of means, permitting direct control over molecular-scale movements within MIMs. These unique molecular machines based on MIMs working in concert have been incorporated into drug-delivery vehicles,[60–66] electrochromic systems,[19,67–70] and molecular electronic devices.[26,55,71–78]

Switchable rotaxanes are particularly well-suited for use as artificial muscles because of the potential to harness the collective efforts of ensembles of linear molecules to exert linear forces, as opposed to catenanes, which exhibit radial motions. These types of molecules can be designed to expand or to contract linearly in response to different stimuli, such as chemical,[18,79–83] electrochemical,[84–88] and optical stimuli.[20,21,89–92] Depending on the design (*vide infra*), switchable rotaxanes are capable of contracting up to 67% of their initial (extended) length,[93–95] suggesting that artificial molecular muscles could be harnessed by tethering to a solid support to perform macroscale work. This section describes recent advances and future prospects for controlling the artificial molecular muscles on both single-molecule and microscopic levels and developing them into nanomechanical devices.[93–99]

One strategy for the development of artificial muscles based on MIMs utilizes hydrogen bonding interactions between a neutral crown ether (dibenzo[24]crown-8, DB24C8) and dibenzylammonium ($R_2NH_2^+$) and bipyridinium ($bypm^{2+}$) stations to produce a pH-switchable system.[18,96] This system has been incorporated[97] into the design of bistable [$c2$]daisy chains, in which two mechanically interlocked filaments glide along one another through the macrocycles (Figure 4). Under acidic conditions, the DB24C8 ring predominantly encircles the dibenzylammonium ion center. In this state, the end-to-end length of a single molecule is approximately 3.1 nm. However, when the $R_2NH_2^+$ center is deprotonated (with the addition of a base), the DB24C8 ring moves from the now-neutral amine site to the dicationic $bypm^{2+}$ site, a consequence of the substantially reduced affinity between the DB24C8 ring and the resulting neutral R_2NH functionality. Under these alkaline conditions, the molecules contract to roughly 2.2 nm (i.e., contracting 30% of the original length). Upon reprotonation of the R_2NH function, the DB24C8 ring reverts from being associated with the $bypm^{2+}$ unit to

encircling the stronger of the two binding sites, namely $R_2NH_2^+$. Analysis of these molecular movements—by proton nuclear magnetic resonance and ultraviolet/visible light absorption spectroscopies—demonstrated quantitative, fully reversible contraction/extension behavior. These results indicate that the molecular movement of this pH-switchable molecule translates into controlled molecule contraction and expansion, reminiscent of the action of muscle filaments.

In addition to these pH-switchable molecular muscles, artificial muscles based on bistable donor-acceptor rotaxanes—designed to undergo actuation in response to chemical and electrochemical stimuli (Figure 5)—have also been developed. These doubly bistable [3]-rotaxanes employ the intramolecular recognition between the π-electron poor tetracationic macrocycle cyclobis (paraquat-*p*-phenylene) (CBPQT⁴⁺) and two π-electron-rich stations, namely naphthalene (NP) and redox-active tetrathiafulvalene (TTF). In unoxidized rotaxane molecules, the encircling CBPQT⁴⁺ is stationed on the neutral TTF unit. When the TTF is oxidized to either the radical TTF•⁺ or dicationic TTF²⁺, the affinity between it and the CBPQT⁴⁺ ring is destroyed, and the ring moves to the weaker alternate NP station. This mechanical movement is

accelerated by the introduction of electrostatic repulsive forces between the mono- or dicationic TTF and the CBPQT⁴⁺ ring. Because of the affinity between the alternative NP station and the CBPQT⁴⁺, subsequent reduction of the TTF does not immediately return the ring to its original state (i.e., the CBPQT⁴⁺ ring located on the neutral TTF unit). The lifetime of this metastable state varies in different environments, depending on matrix effects,[98] indicating that the doubly bistable [3]rotaxane can persist in this metastable (actuated) state long after the electrochemical stimulus is removed.

Palindromic rotaxanes incorporating the bistable (TTF-DNP-CBPQT⁴⁺) motif were designed as molecular analogues to skeletal muscles that could "expand" and "contract" linearly in response to chemical or electrochemical stimuli. The prototypical design[94] (Figure 5) contains two CBPQT⁴⁺ rings that are located on the TTF stations approximately 4.2 nm apart from each other (Figure 5a, upper diagram). Oxidation of the molecule introduces electrostatic repulsion between TTF²⁺ stations and the CBPQT⁴⁺ rings that force the macrocycles to move to the more favorable DNP (dioxynaphthalene) stations, placing the rings effectively 1.4 nm apart (Figure 5a, lower diagram). This movement represents approximately a 67% contraction of
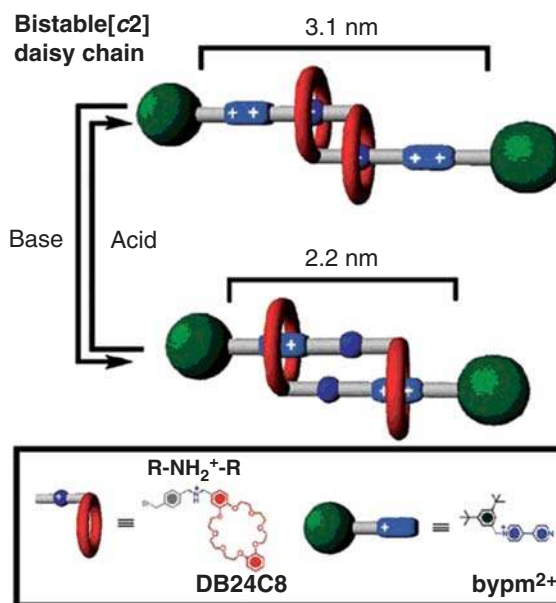

Figure 4. Schematic representation of a [$c2$]daisy chain illustrating the assembly and anticipated mechanical motions of this pH-switchable and fully reversible molecular muscle system. Under acidic conditions, the end-to-end distance of a single molecule is on the order of 3.1 nm. The addition of base stimulates rearrangement of the molecule into a 30% shorter contracted state. DB24C8, dibenzo[24]crown-8; $R_2NH_2^+$, dibenzylammonium; $bypm^{2+}$, bipyridinium. Reprinted with permission from Reference 97. ©2008, Wiley-VCH Verlag GmbH & Co. KGaA.
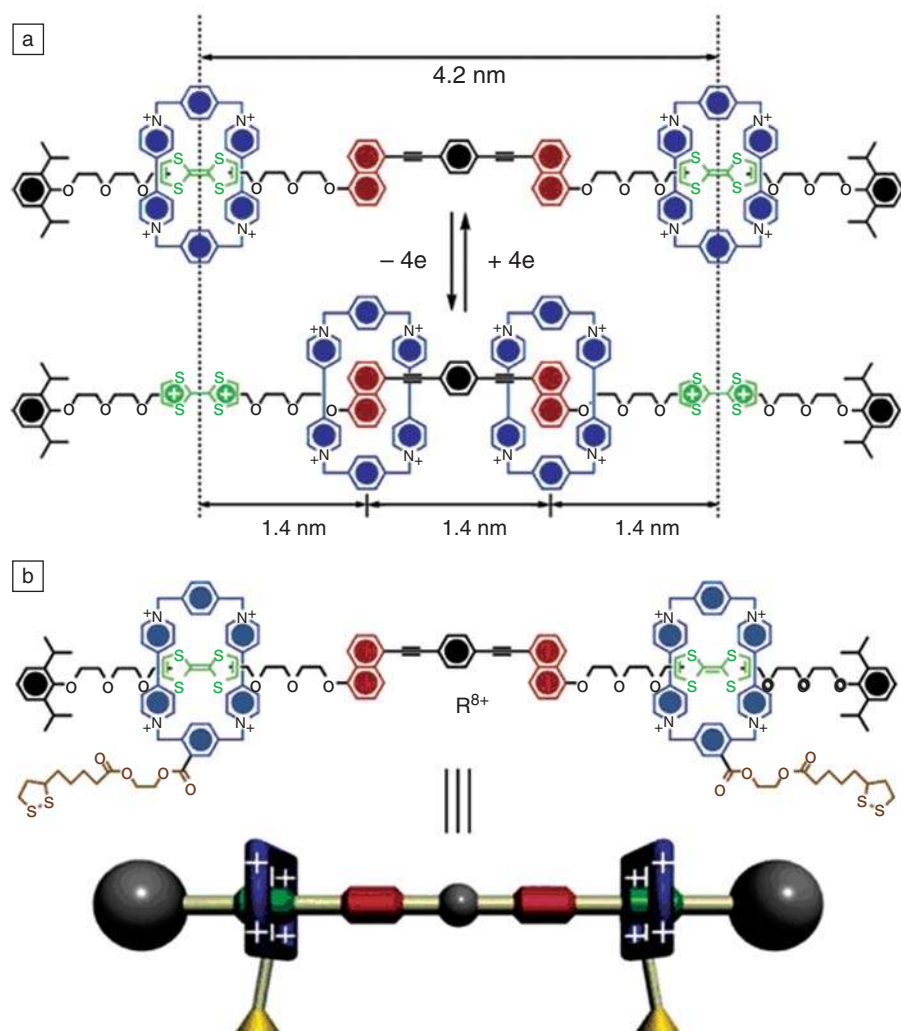
Figure 5. (a) Structural formulas of the extended (top) and the contracted (bottom) states of a prototypical molecular muscle based on doubly bistable [3]rotaxanes. In the relaxed state, cyclobis(paraquat-p-phenylene) (CBPQT^{4+}) rings (blue) encircle the electron-rich tetrathiafulvalene (TTF) stations (green), approximately 4.2 nm apart. With chemical or electrochemical oxidation of TTF stations, CBPQT^{4+} rings move inward to the secondary naphthalene (NP) stations (red), approximately 1.4 nm apart, effecting a 67% reduction in distance between CBPQT^{4+} rings (blue). (b) Structural formula and graphical representation of a disulfide-tethered bistable molecular muscle used in subsequent cantilever bending experiments. Reprinted with permission from Reference 94. ©2005, American Chemical Society.

molecule of approximately 10 pN. Furthermore, this significant deflection was reversible and bent downward with the addition of a reducing agent (ascorbic acid), an observation consistent with the reversible switching of the bistable muscle molecules. This reversibility, repeated for up to 25 cycles (Figure 6), was limited by the degradation of either the gold-thiol bond or the rotaxane itself. These experiments indicate that the collective action of appropriately designed individual rotaxane molecules that are tethered to surfaces can indeed perform macroscale work.

The action of these surface-tethered molecular muscles can also be controlled electrochemically.[95] In this case, the gold-coated microcantilever was used as a working electrode in a modified three-electrode electrochemical cell. When the potential of the cantilever was held at a level high enough to oxidize the TTF station but low enough to prevent oxidation of the Au-S linkages (0.4 V versus Ag/AgCl in 0.1 M aqueous $NaClO_4$), a dramatic deflection of the cantilever occurred, a consequence of the mechanical stress applied to the cantilever by the contraction of the muscle molecules. Furthermore, reducing the potential to one that is capable of reducing the oxidized TTF but not low enough to reduce the CBPQT^{4+} ring caused the cantilever to relax. This electrochemically induced contraction/relaxation was also partially reversible (Figure 6c).

As described earlier, rotaxanes introduce many important avenues of current research aimed toward the design and control of artificial molecular muscles. The pH-switchable [c2]daisy chain molecules are readily amenable to modification with carefully chosen functional groups. This modification would enable future work toward incorporating these types of pH-switchable muscle molecules into cantilever devices and the production of functionalized muscle molecules that could be incorporated into liquid crystalline[68] or polymeric[100] systems. The material properties of these networked MIMs would then be responsive to changes in pH at the monomeric level. Furthermore, mechanical devices that incorporate doubly bistable [3]rotaxanes represent significant advances over previous approaches toward artificial muscle systems based on molecular machines. The opportunity exists now to tackle other key objectives. Chief among them is preventing the degradation of muscle molecules to enable truly reversible macroscale behavior and longer device lifetimes. Current work is focused on improving the device fabrica-
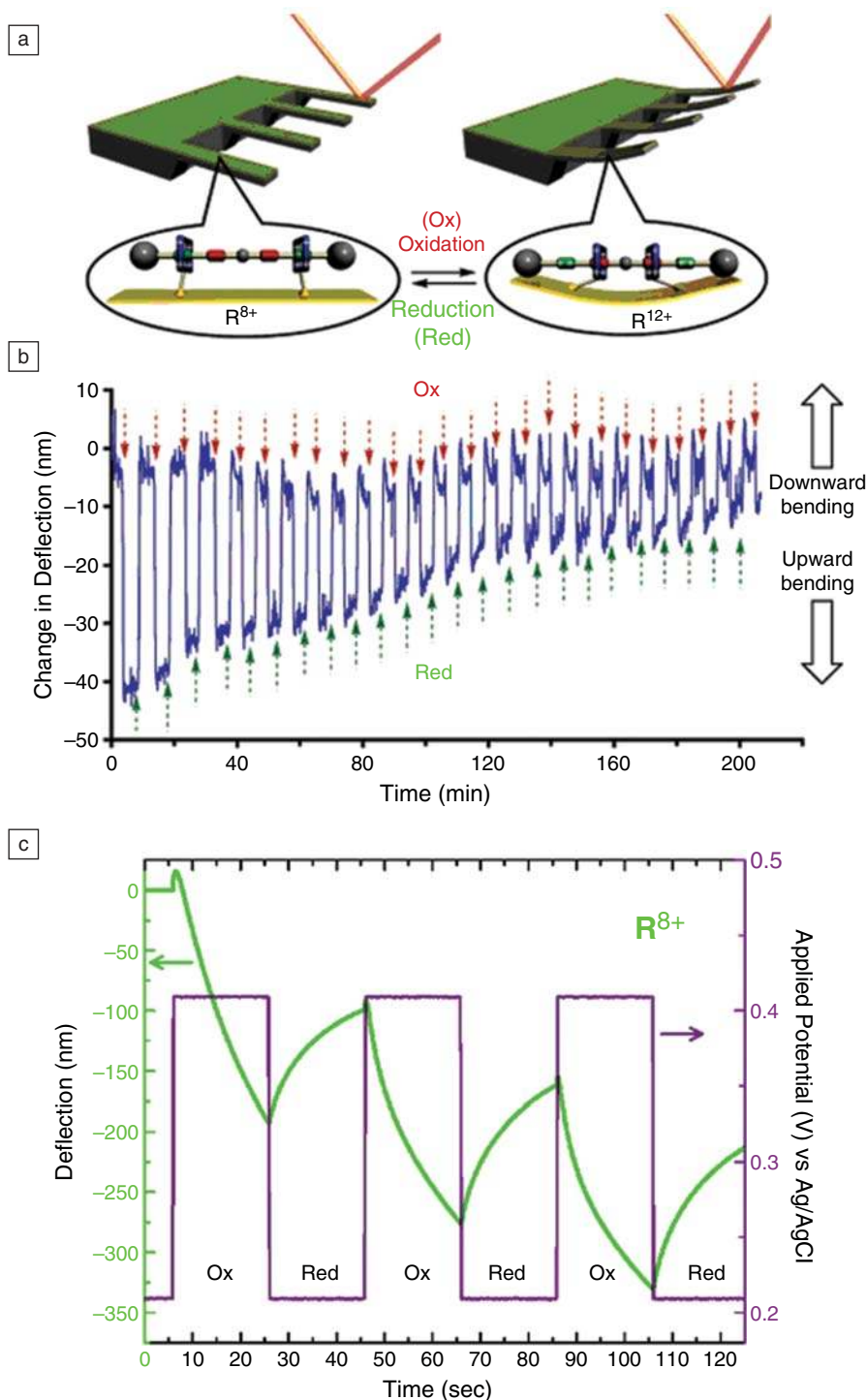
the distance between the two rings. By incorporating disulfides into these palindromic rotaxanes (i.e., on the CBPQT^{4+} rings) these molecules can be coupled to gold surfaces. This design element allows the relative motions of the ring components in the bistable [3]rotaxanes to be coupled mechanically to the surface, an important step in harnessing molecular machines to perform macroscale work.

These redox-active rotaxanes have already made their way from the laboratory flask to the surfaces of microcantilevers with the aim of measuring the collective work performed by ensembles of molecules working in concert.[93–95,99] Self-assembled monolayers composed of approximately six billion randomly aligned symmetrical rotaxanes were covalently attached to a thin film of gold (via gold-thiol chemistry) coated onto one side of silicon cantilevers.[93,94] These cantilevers bent when exposed to an oxidizing agent (Fe(ClO$_4$)$_3$) in response to the oxidation of TTF stations and subsequent contraction of the individual rotaxane molecules. The observed deflection (35 nm) corresponds to a linear force per

675

Figure 6. (a) Schematic diagram of the proposed mechanism for the operation of a molecular muscle device. R^{12+} is the oxidized form of R^{8+} (shown in Figure 5b), where both of the tetrathiafulvalene stations are oxidized to dicationic TTF^{2+} (as in Figure 5a). (b) Time series of deflection data showing 25 cycles of chemical oxidation and reduction of molecular muscles on a gold cantilever inducing the upward and downward deflections of one cantilever beam coated with palindromic bistable [3]rotaxane R^{8+}. Reprinted with permission from Reference 94. ©2005, American Chemical Society. (c) The deflection versus time (green line) of a gold cantilever coated with R^{8+} when subjected to a series of oxidation and reduction potential steps (purple line). Reprinted with permission from Reference 95. ©2009, American Chemical Society.

tion conditions—particularly related to the preparation of self-assembled monolayers on cantilevers—and incorporating passivating layers around the active device components.

Carbon Nanotube–Based Artificial Muscles

Carbon nanotubes have likely provided more fundamentally different types of actuators than any other material type. Electrostatic attraction and repulsion between two nanotubes have been used for cantilever-based nano-tweezers[101] and mechanically based switches and logic elements.[102,103] On the macroscale, electrically powered[104–111] and fuel-powered[112,113] electrochemical carbon nanotube actuators provide up to a few percent actuator stroke and over a hundred times higher stress generation than natural muscle. Large-stroke pneumatic nanotube actuators have been demonstrated that use electrochemical gas generation within nanotube sheets.[114] Carbon nanotubes also have been used as additives that act in conjunction with organic polymers to provide photoresponsive,[115] shape memory,[116,117] and electromechanical[118] actuators.

Since carbon nanotubes are prototypical materials that can support much higher mechanical loads than is possible for other low density actuator materials having the same cross-sectional area, we focus on electrically driven and fuel-driven artificial muscles based on carbon nanotube sheets and yarns. Whether electrically or chemically driven, these actuators use dimensional changes resulting from electrochemical charge injection into nanotubes or nanotube bundles. While other carbon nanotube types could be used, exploited carbon nanotubes are of the simplest types, either carbon single-wall nanotubes (SWNTs) or multiwall nanotubes (MWNTs). A SWNT can be viewed heuristically as a single sheet of graphite that has been rolled about an axis to make a seamless cylinder having a nanoscale diameter. Integer n and m indices (n, m) denote the axis of rolling with respect to crystallographic directions of the graphite sheet.[119] When either n or m is 0, the nanotubes are called "zigzag," since cyclic rings of carbon atoms around the circumference of the nanotube have a zigzag arrangement. If $n = m$, the nanotubes are called "armchair," since the cyclic carbon-carbon chains have connecting bonds that alternate between being parallel and inclined with respect to the circumference. Otherwise, the nanotubes are called "chiral," since the carbon chains form either left- or right-handed helices. These indices

profoundly affect actuation at low degrees of charge injection, as well as diverse nanotube electronic and optical properties. MWNTs are composed of nested SWNTs with increasing diameters, forming concentric cylinders, such as the rings of a tree trunk.

Several billion miles of individual 10-nm diameter, nine-wall MWNTs must be assembled for each pound of carbon nanotube actuator material, and the required length per pound increases with decreasing outer diameter and number of walls for the nanotube (corresponding to decreasing weight per length of the nanotubes). Though major advances have been made in such nanotube assembly to make long yarns and sheets,[120–125] achieved strengths, stiffnesses, and creep resistance are still far below the spectacular mechanical properties demonstrated[126] for individual SWNTs. This discrepancy between measured mechanical properties of individual nanotubes and those of nanotube sheets and yarns is principally caused by poor stress transfer between nanotube bundles, outer and inner nanotubes in nanotube bundles, and outer and inner walls of MWNTs. In all cases, this stress transfer can be improved by increasing the nanotube length.

Due to both the high degree of nanotube alignment that can be obtained and applicability to ultralong nanotubes, a solid-state process is especially attractive for further development for the production of both carbon nanotube yarns and sheets. This process starts from forests of carbon nanotubes, which comprise approximately parallel nanotubes that are arrayed like the trees in a bamboo forest, that are made by chemical vapor deposition. Yarns and sheets are mechanically drawn from these forests, and yarn twist can be introduced during draw using a nanosized version of conventional twist-based spinning (Figure 7a–c).[121,122]

Carbon Nanotube Muscles Based on Electrical or Chemical Double-Layer Charge Injection

Electrochemical charge injection-based carbon nanotube muscles were initially proposed in 1996[127] and experimentally demonstrated three years later.[104] Similar to electrochemical conducting polymer muscles, which were first described in 1990[127,128] and remain the subject of research and commercialization activities, these carbon nanotube muscles function as the working electrode (or both the working and counter electrodes) in an electrochemical cell (Figure 8a and 8b). Actuating electrodes in conducting polymer muscles operate by Faradaic

processes and are essentially battery electrodes; dopant intercalation and deintercalation provide the dimensional changes needed for actuation. On the other hand, carbon nanotube artificial muscle electrodes use non-Faradaic processes by undergoing double-layer charge injection, as for electrochemical supercapacitors. Since dopant intercalation is not required, artificial muscles that expand and contract by supercapacitor charging can have a longer cycle life than those that utilize Faradaic charging.

Due to the high surface-to-volume ratios of carbon nanotubes and the nanometer-scale distances between injected electronic

charges and compensating ionic charges, the capacitance of nanotube-based electrodes is in the range of ~15 to 200 F/g,[126] depending on the surface areas of the nanotube assembly and the electrolyte. This means that application of a few volts can produce a large amount of charge injection and corresponding mechanical deformation of nanotubes, compared to the high operating voltages (hundreds of volts) needed to produce comparable actuator strains for conventional high-modulus ferroelectric actuators. Since electrode intercalation and deintercalation are not required (these are slow and only partially reversible for conducting polymer
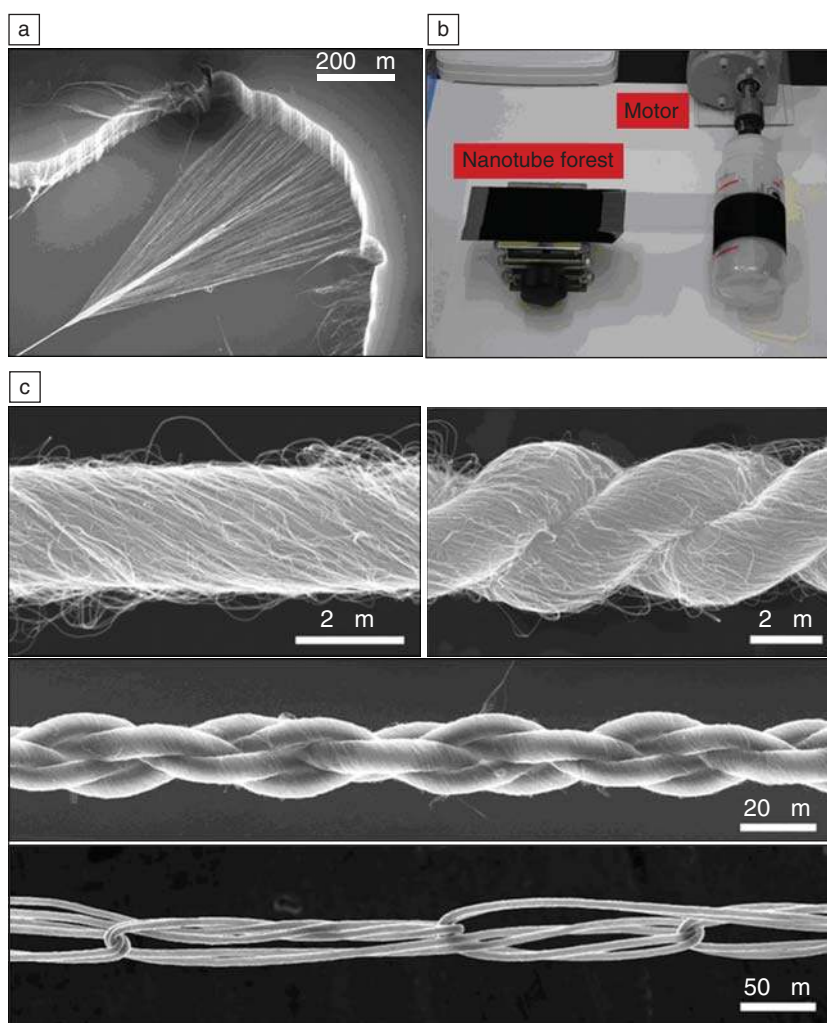

Figure 7. (a) Scanning electron microscopy (SEM) images showing a carbon nanotube yarn being fabricated by simultaneously being drawn and twisted during spinning from a vertically aligned multiwall nanotube (MWNT) forest. (b) Photograph showing a carbon nanotube sheet being drawn from a nanotube forest and wrapped on a rotating mandrel. (c) SEM images of single-ply MWNT yarn made by the process of (a) and two-ply, four-ply, and knitted MWNT yarns made from such single-ply yarn. (a) and (c) are reprinted with permission from Reference 121. ©2004, American Association for the Advancement of Science.

muscles), the carbon nanotube muscles have advantages over conducting polymer muscles in both actuation rate and device lifetime. Madden et al.[107] demonstrated a stroke rate of 19% s^{-1} and an instantaneous power density of 270 W kg^{-1} for a carefully designed carbon nanotube muscle, which exceeds the stroke rate and power density of human skeletal muscle. Comparable strain rates (12% s^{-1}) and power densities (150 W kg^{-1}) have been obtained for conducting polymer artificial muscles.[129] The highest strain rate observed for any artificial muscle is a spectacular 3.7×10^{4}% s^{-1} for carbon nanotube artificial muscles that are capacitively driven by charge injection in the absence of an electrolyte, which provide strokes above 220% and can operate between at least the demonstrated 80 and 1900 K.[130] However, these newest carbon nanotube artificial muscles require the application of kilovolts to achieve such giant strains.

The performance of carbon nanotube artificial muscles has dramatically increased with improvement in the mechanical properties of carbon nanotube sheets and yarns. For the initially demonstrated carbon nanotube actuators (which used the then-available unoriented filtration-produced nanotube sheets with low modulus and strength), actuator stroke (0.2%) was about the same as for high modulus ferroelectric actuators, and the generated isometric stress was only ~1 MPa.[104] Using more recently available highly oriented carbon nanotube yarns that have much higher modulus and strength, this actuation stress was increased to 26 MPa, which is nearly a hundred times that of natural muscle.[107,108,126] This stress generation capability (whose product with the muscle cross-sectional area determines the maximum weight that an initially unloaded muscle can lift) is still far below the ultimate potential of carbon nanotube artificial muscles, which could be achieved by increasing the modulus of carbon nanotube yarns to close to that of the individual carbon nanotubes. Using the ~0.2% strain that is typically observed for carbon nanotube yarns and sheets[108] and a 640 GPa Young's modulus,[126] an isometric stress generation capability potentially of 1.3 GPa (which is the product of the strain and modulus) could be generated by SWNT actuators, which is about 4000 times higher than that of natural muscle. If the stroke of natural muscle is needed, this 0.2% strain must be amplified to about 20%, which will decrease the stress generation capability of the artificial muscle to about a 40 times higher value than natural muscle. However, these nanotube artificial muscles are unlikely to replace natural muscle in the human body. Even ignoring possible safety issues, the stroke capabilities of the described artificial muscles are too low, and the complexities of amplifying these strokes to match those of natural muscles are too great.

The origin of the dimensional changes that cause actuator stroke during double-layer charge injection is complicated and incompletely understood. Quantum chemical effects are important at low degrees of charge injection, and these effects are quite different for nanotubes having different (n, m) indices.[131,132] When SWNT diameters are small, the fractional change in length and diameter resulting from charge injection oscillates greatly but predictably in amplitude depending upon whether $|n - m|$ deviates from a multiple of three by 0, 1, or 2. These oscillations can be understood by the differences in the locations of bonding and antibonding orbitals for the different series, since addition of an electron causes bond lengths to contract or to expand depending upon whether the orbital is bonding or antibonding, respectively. While the quantum mechanical contribution to length expansion caused by electron injection is maximized for nanotubes, where $|n - m|$ deviates from a multiple of 3 by 2, present SWNTs used for actuation are not selected according to nanotube type. This lack of optimization degrades the actuation achieved for low degrees of charge injection.

The quantum mechanical contribution to actuation varies at low degrees of charge injection as q, where q is the amount of injected charge. At higher degrees of charge injection, actuation is dominated by electrostatic effects, which are approximately proportional to q^2. The observed quadratic contribution to actuation from coulombic repulsion can be derived (by approximating the electrode capacitance as potential-independent and by approximating the fiber-direction Young's modulus (Y) as the appropriate effective modulus) using the Lippmann equation: $d\gamma/dV = -q_a$, which relates the charge per unit surface area of the actuating material (q_a) to the derivative of surface energy (γ) with respect to the electrode potential (V). The result is that the electrostatic contribution to change of length (L) of individual nanofibers (individual nanotubes or nanotube bundles) is approximately

$$\Delta L / L = 1/2 \, q_a^2 R/C_a, \qquad (1)$$

where R is the surface-to-volume ratio for the nanofiber and C_a is the capacitance per electrochemically accessible surface area of the nanotube electrode.

The existence of repulsion between double layers on different nanotubes (or, more usually, nanotube bundles) provides an additional electrostatic effect that can increase nanotube yarn or sheet actuation. The resulting actuator stroke inversely depends on the macroscopic stiffness instead of the much larger nanoscale stiffness of the individual nanotubes, which can increase the magnitude of actuation for low modulus nanotube assemblies. Repulsion between double layers likely explains the cantilever-based actuation observed upon electrochemical double-layer-charge-injection of sheet strip electrodes comprising carbon nanotube forest electrodes that had been transferred from the Si growth substrate to a flexible gold foil substrate.[110]

Fuel-powered carbon nanotube artificial muscles also operate electrochemically by double-layer-charge-injection using fuels such as hydrogen, formic acid,
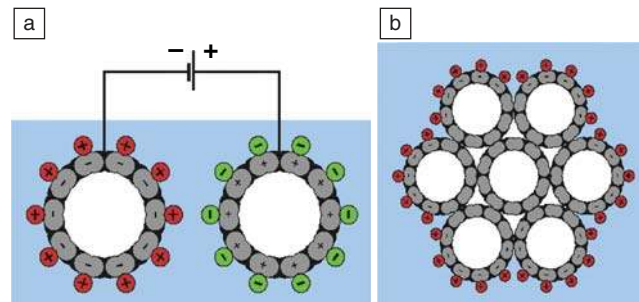

Figure 8. (a and b) Schematic illustrations of charge injection in carbon-nanotube-based electromechanical actuators. Nanotubes or nanotube assemblies are submerged into an electrolyte and form an electrochemical cell with the nanotubes as electrodes. Application of a potential injects electronic charges of opposite signs in the two nanotube electrodes, which is balanced by ionic charge near the surfaces of (a) single nanotubes and (b) a nanotube bundle. Reprinted with permission from Reference 104. ©1999, American Association for the Advancement of Science.

or methanol. This time, the actuating carbon nanotube electrodes simultaneously function as fuel cell electrodes to convert chemical energy to electrical energy in the form of stored charge, as supercapacitor electrodes to store this charge, and as actuators that convert changes in stored charge to actuator stroke.[112,113]

The exploitation of charge-injection-based carbon nanotubes for highly reversible, high-cycle-life muscles requires the elimination of a major problem—irreversible plastic deformation occurring under high load conditions, which increases the strain obtained at a provided electrode potential. The strain rate of this plastic deformation, which depends on electrode potential and the mechanical load on the muscle, has recently been substantially decreased through the use of solid-state fabricated twisted nanotube yarns containing ~300-μm long carbon nanotubes.[108] We expect that major increases in nanotube length will eliminate this problem by increasing inter-nanotube stress transfer.

Actuator stroke for charge-injection-based nanotube actuators can be increased by decreasing the numbers of nanotubes in a bundle, thereby increasing electrode gravimetric capacitance and the degree of charge injection for a given applied potential (Figure 8a and 8b). Also, the quantum mechanical contribution to actuation can be increased through the use of nanotube types that optimize charge-induced nanotube expansion. Energy conversion efficiency (presently below 1% for nanotube yarns), force generation capability, and power generation capability are presently limited by imperfect coupling of forces generated on the nanotube level to provide yarn- or sheet-level forces that enable external mechanical work. All of these performance characteristics will continue to improve as nanotube yarn strength and modulus begin to approach those of the component nanotubes.

Summary and Prospects

We have discussed three proven examples of nanomechanical actuation in artificial molecular systems, ranging from single-molecule switches to supramolecular rotaxane motors to carbon nanotube-based artificial muscles. These examples illustrate a number of key advances in exploring single molecules and nano-scale architectures as building blocks for fabrication of functional molecular-scale machines. Understanding induced molecular motion as a result of external stimuli provides insight into the nanomechanical properties of single molecules, supramolecular assemblies, and hierarchically assembled structures. Combining this understanding of molecular behavior with advances in self- and directed assembly techniques paves the way toward novel nanomechanical machines. Ultimately, the ability to integrate these molecular machines functionally and to multiplex them for macroscale work will facilitate the development of multifunctional devices that can mimic and potentially surpass the complicated functions of natural systems.

References

1. C. Joachim, J.K. Gimzewski, A. Aviram, *Nature* **408**, 541 (2000).
2. V. Balzani, A. Credi, F.M. Raymo, J.F. Stoddart, *Angew. Chem. Int. Ed.* **39**, 3349 (2000).
3. P.S. Weiss, *Acc. Chem. Res.* **41**, 1772 (2008).
4. R.A. Bissell, E. Cordova, A.E. Kaifer, J.F. Stoddart, *Nature* **369**, 133 (1994).
5. C.M. Niemeyer, *Appl. Phys. A* **68**, 119 (1999).
6. M. Gomez-Lopez, J.A. Preece, J.F. Stoddart, *Nanotechnology* **7**, 183 (1996).
7. A.P. Alivisatos, *Science* **271**, 933 (1996).
8. D.L. Klein, R. Roth, A.K.L. Lim, A.P. Alivisatos, P.L. McEuen, *Nature* **389**, 699 (1997).
9. Y. Cui, C.M. Lieber, *Science* **291**, 851 (2001).
10. X.F. Duan, Y. Huang, Y. Cui, J.F. Wang, C.M. Lieber, *Nature* **409**, 66 (2001).
11. Y. Huang, X.F. Duan, Y. Cui, L.J. Lauhon, K.H. Kim, C.M. Lieber, *Science* **294**, 1313 (2001).
12. A. Bachtold, P. Hadley, T. Nakanishi, C. Dekker, *Science* **294**, 1317 (2001).
13. Y.H. Lee, Y.T. Jang, C.H. Choi, D.H. Kim, C.W. Lee, J.E. Lee, Y.S. Han, S.S. Yoon, J.K. Shin, S.T. Kim, E.K. Kim, B.K. Ju, *Adv. Mater.* **13**, 1371 (2001).
14. V. Derycke, R. Martel, J. Appenzeller, P. Avouris, *Nano Lett.* **1**, 453 (2001).
15. C. Dekker, *Phys. Today* **52**, 22 (1999).
16. S.J. Tans, A.R.M. Verschueren, C. Dekker, *Nature* **393**, 49 (1998).
17. V. Balzani, A. Credi, M. Venturi, Eds., *Molecular Devices and Machines: Concepts and Perspectives for the Nanoworld*, Second edition (Wiley-VCH, Weinheim, 2008).
18. A.M. Elizarov, S.H. Chiu, J.F. Stoddart, *J. Org. Chem.* **67**, 9175 (2002).
19. T. Ikeda, S. Saha, I. Aprahamian, K.C.F. Leung, A. Williams, W.Q. Deng, A.H. Flood, W.A. Goddard, J.F. Stoddart, *Chem. Asian J.* **2**, 76 (2007).
20. R. Ballardini, V. Balzani, M.T. Gandolfi, L. Prodi, M. Venturi, D. Philp, H.G. Ricketts, J.F. Stoddart, *Angew. Chem. Int. Ed.* **32**, 1301 (1993).
21. S. Saha, J.F. Stoddart, *Chem. Soc. Rev.* **36**, 77 (2007).
22. A. Credi, M. Venturi, *Cent. Eur. J. Chem.* **6**, 325 (2008).
23. A.S. Kumar, T. Ye, T. Takami, B.C. Yu, A.K. Flatt, J.M. Tour, P.S. Weiss, *Nano Lett.* **8**, 1644 (2008).
24. A.P. de Silva, S. Uchiyama, *Nat. Nanotechnol.* **2**, 399 (2007).
25. B. Yurke, A.J. Turberfield, A.P. Mills, F.C. Simmel, J.L. Neumann, *Nature* **406**, 605 (2000).
26. B.A. Mantooth, P.S. Weiss, *Proc. IEEE* **91**, 1785 (2003).
27. A.M. Moore, P.S. Weiss, *Annu. Rev. Anal. Chem.* **1**, 857 (2008).
28. C. Joachim, M.A. Ratner, *Proc. Nat. Acad. Sci. U.S.A.* **102**, 8801 (2005).
29. D.J. Fuchs, P.S. Weiss, *Nanotechnology* **18**, 044021 (2007).
30. T.D. Dunbar, M.T. Cygan, L.A. Bumm, G.S. McCarty, T.P. Burgin, W.A. Reinerth, L. Jones, J.J. Jackiw, J.M. Tour, P.S. Weiss, D.L. Allara, *J. Phys. Chem. B* **104**, 4880 (2000).
31. L.A. Bumm, J.J. Arnold, M.T. Cygan, T.D. Dunbar, T.P. Burgin, L. Jones, D.L. Allara, J.M. Tour, P.S. Weiss, *Science* **271**, 1705 (1996).
32. J.M. Seminario, A.G. Zacarias, J.M. Tour, *J. Am. Chem. Soc.* **122**, 3015 (2000).
33. J.M. Seminario, C.E. De la Cruz, P.A. Derosa, *J. Am. Chem. Soc.* **123**, 5616 (2001).
34. J.M. Seminario, A.G. Zacarias, J.M. Tour, *J. Am. Chem. Soc.* **120**, 3970 (1998).
35. J.M. Tour, *Chem. Rev.* **96**, 537 (1996).
36. M. Di Ventra, S.G. Kim, S.T. Pantelides, N.D. Lang, *Phys. Rev. Lett.* **86**, 288 (2001).
37. L.A. Bumm, J.J. Arnold, L.F. Charles, T.D. Dunbar, D.L. Allara, P.S. Weiss, *J. Am. Chem. Soc.* **121**, 8017 (1999).
38. R.K. Smith, P.A. Lewis, P.S. Weiss, *Prog. Surf. Sci.* **75**, 1 (2004).
39. Z.J. Donhauser, B.A. Mantooth, K.F. Kelly, L.A. Bumm, J.D. Monnell, J.J. Stapleton, D.W. Price, A.M. Rawlett, D.L. Allara, J.M. Tour, P.S. Weiss, *Science* **292**, 2303 (2001).
40. M.T. Cygan, T.D. Dunbar, J.J. Arnold, L.A. Bumm, N.F. Shedlock, T.P. Burgin, L. Jones, D.L. Allara, J.M. Tour, P.S. Weiss, *J. Am. Chem. Soc.* **120**, 2721 (1998).
41. M. Weck, J.J. Jackiw, R.R. Rossi, P.S. Weiss, R.H. Grubbs, *J. Am. Chem. Soc.* **121**, 4088 (1999).
42. A.M. Moore, B.A. Mantooth, A.A. Dameron, Z.J. Donhauser, P.A. Lewis, R.K. Smith, D.J. Fuchs, P.S. Weiss, *Adv. Mater. Res.* **10**, 29 (2008).
43. P.A. Lewis, C.E. Inman, Y.X. Yao, J.M. Tour, J.E. Hutchison, P.S. Weiss, *J. Am. Chem. Soc.* **126**, 12214 (2004).
44. T.J. Mullen, C. Srinivasan, J.N. Hohman, S.D. Gillmor, M.J. Shuster, M.W. Horn, A.M. Andrews, P.S. Weiss, *Appl. Phys. Lett.* **90**, 063114 (2007).
45. T.J. Mullen, A.A. Dameron, A.M. Andrews, P.S. Weiss, *Aldrichim. Acta* **40**, 21 (2007).
46. L.A. Bumm, J.J. Arnold, T.D. Dunbar, D.L. Allara, P.S. Weiss, *J. Phys. Chem. B* **103**, 8122 (1999).
47. X.D. Cui, A. Primak, X. Zarate, J. Tomfohr, O.F. Sankey, A.L. Moore, T.A. Moore, D. Gust, G. Harris, S.M. Lindsay, *Science* **294**, 571 (2001).
48. A.M. Moore, B.A. Mantooth, Z.J. Donhauser, F. Maya, D.W. Price, Y.X. Yao, J.M. Tour, P.S. Weiss, *Nano Lett.* **5**, 2292 (2005).
49. J.M. Tour, *Acc. Chem. Res.* **33**, 791 (2000).
50. J.M. Tour, A.M. Rawlett, M. Kozaki, Y.X. Yao, R.C. Jagessar, S.M. Dirk, D.W. Price, M.A. Reed, C.W. Zhou, J. Chen, W.Y. Wang, I. Campbell, *Chem. Eur. J.* **7**, 5118 (2001).

51. P.A. Lewis, C.E. Inman, F. Maya, J.M. Tour, J.E. Hutchison, P.S. Weiss, *J. Am. Chem. Soc.* **127**, 17421 (2005).

52. M. Magoga, C. Joachim, *Phys. Rev. B* **56**, 4722 (1997).

53. P.A. Derosa, J.M. Seminario, *J. Phys. Chem. B* **105**, 471 (2001).

54. P.A. Lewis, Z.J. Donhauser, B.A. Mantooth, R.K. Smith, L.A. Bumm, K.F. Kelly, P.S. Weiss, *Nanotechnology* **12**, 231 (2001).

55. A.M. Moore, A.A. Dameron, B.A. Mantooth, R.K. Smith, D.J. Fuchs, J.W. Ciszek, F. Maya, Y.X. Yao, J.M. Tour, P.S. Weiss, *J. Am. Chem. Soc.* **128**, 1959 (2006).

56. A.A. Dameron, J.W. Ciszek, J.M. Tour, P.S. Weiss, *J. Phys. Chem. B* **108**, 16761 (2004).

57. J.F. Stoddart, H.R. Tseng, *Proc. Nat. Acad. Sci. U.S.A.* **99**, 4797 (2002).

58. K.E. Griffiths, J.F. Stoddart, *Pure Appl. Chem.* **80**, 485 (2008).

59. F. Diederich, P.J. Stang, Eds., *Templated Organic Synthesis*. (Wiley-VCH, Weinheim, 1999).

60. T.D. Nguyen, H.R. Tseng, P.C. Celestre, A.H. Flood, Y. Liu, J.F. Stoddart, J.I. Zink, *Proc. Nat. Acad. Sci. U.S.A.* **102**, 10029 (2005).

61. T.D. Nguyen, Y. Liu, S. Saha, K.C.F. Leung, J.F. Stoddart, J.I. Zink, *J. Am. Chem. Soc.* **129**, 626 (2007).

62. T.D. Nguyen, K.C.-F. Leung, M. Liong, C.D. Pentecost, J.F. Stoddart, J.I. Zink, *Org. Lett.* **8**, 3363 (2006).

63. S. Saha, K.C.-F. Leung, T.D. Nguyen, J.F. Stoddart, J.I. Zink, *Adv. Funct. Mater.* **17**, 685 (2007).

64. S. Angelos, E. Johansson, J.F. Stoddart, J.I. Zink, *Adv. Funct. Mater.* **17**, 2261 (2007).

65. S. Angelos, Y.-W. Yang, K. Patel, J.F. Stoddart, J.I. Zink, *Angew. Chem. Int. Ed.* **47**, 2222 (2008).

66. K. Patel, S. Angelos, W.R. Dichtel, A. Coskun, Y.-W. Yang, J.I. Zink, J.F. Stoddart, *J. Am. Chem. Soc.* **130**, 2382 (2008).

67. D.W. Steuerman, H.R. Tseng, A.J. Peters, A.H. Flood, J.O. Jeppesen, K.A. Nielsen, J.F. Stoddart, J.R. Heath, *Angew. Chem. Int. Ed.* **43**, 6486 (2004).

68. I. Aprahamian, T. Yasuda, T. Ikeda, S. Saha, W.R. Dichtel, K. Isoda, T. Kato, J.F. Stoddart, *Angew. Chem. Int. Ed.* **46**, 4675 (2007).

69. W.Q. Deng, A.H. Flood, J.F. Stoddart, W.A. Goddard, *J. Am. Chem. Soc.* **127**, 15994 (2005).

70. T. Ikeda, I. Aprahamian, J.F. Stoddart, *Org. Lett.* **9**, 1481 (2007).

71. J.E. Green, J.W. Choi, A. Boukai, Y. Bunimovich, E. Johnston-Halperin, E. DeIonno, Y. Luo, B.A. Sheriff, K. Xu, Y.S. Shin, H.-R. Tseng, J.F. Stoddart, J.R. Heath, *Nature* **445**, 414 (2007).

72. W.R. Dichtel, J.R. Heath, J.F. Stoddart, *Philos. Trans. R. Soc. London, Ser. A* **365**, 1607 (2007).

73. A.H. Flood, R.J.A. Ramirez, W.Q. Deng, R.P. Muller, W.A. Goddard, J.F. Stoddart, *Aust. J. Chem.* **57**, 301 (2004).

74. A.H. Flood, J.F. Stoddart, D.W. Steuerman, J.R. Heath, *Science* **306**, 2055 (2004).

75. S.S. Jang, Y.H. Jang, Y.H. Kim, W.A. Goddard, J.W. Choi, J.R. Heath, B.W. Laursen, A.H. Flood, J.F. Stoddart, K. Norgaard, T. Bjornholm, *J. Am. Chem. Soc.* **127**, 14804 (2005).

76. Y. Luo, C.P. Collier, J.O. Jeppesen, K.A. Nielsen, E. DeIonno, G. Ho, J. Perkins, H.R. Tseng, T. Yamamoto, J.F. Stoddart, J.R. Heath, *ChemPhysChem* **3**, 519 (2002).

77. A.R. Pease, J.O. Jeppesen, J.F. Stoddart, Y. Luo, C.P. Collier, J.R. Heath, *Acc. Chem. Res.* **34**, 433 (2001).

78. H.R. Tseng, S.A. Vignon, P.C. Celestre, J. Perkins, J.O. Jeppesen, A. Di Fabio, R. Ballardini, M.T. Gandolfi, M. Venturi, V. Balzani, J.F. Stoddart, *Chem. Eur. J.* **10**, 155 (2004).

79. P.R. Ashton, R. Ballardini, V. Balzani, I. Baxter, A. Credi, M.C.T. Fyfe, M.T. Gandolfi, M. Gomez-Lopez, M.V. Martinez-Diaz, A. Piersanti, N. Spencer, J.F. Stoddart, M. Venturi, A.J.P. White, D.J. Williams, *J. Am. Chem. Soc.* **120**, 11932 (1998).

80. J.D. Badjic, V. Balzani, A. Credi, S. Silvi, J.F. Stoddart, *Science* **303**, 1845 (2004).

81. J.D. Badjic, C.M. Ronconi, J.F. Stoddart, V. Balzani, S. Silvi, A. Credi, *J. Am. Chem. Soc.* **128**, 1489 (2006).

82. A.S. Lane, D.A. Leigh, A. Murphy, *J. Am. Chem. Soc.* **119**, 11092 (1997).

83. T.J. Huang, *MRS Bull.* **33**, 226 (2008).

84. R. Ballardini, V. Balzani, J. Becher, A. Di Fabio, M.T. Gandolfi, G. Mattersteig, M.B. Nielsen, F.M. Raymo, S.J. Rowan, J.F. Stoddart, A.J.P. White, D.J. Williams, *J. Org. Chem.* **65**, 4120 (2000).

85. V. Bermudez, N. Capron, T. Gase, F.G. Gatti, F. Kajzar, D.A. Leigh, F. Zerbetto, S.W. Zhang, *Nature* **406**, 608 (2000).

86. J.P. Collin, P. Gavina, J.P. Sauvage, *New J. Chem.* **21**, 525 (1997).

87. S. Nygaard, K.C.F. Leung, I. Aprahamian, T. Ikeda, S. Saha, B.W. Laursen, S.Y. Kim, S.W. Hansen, P.C. Stein, A.H. Flood, J.F. Stoddart, J.O. Jeppesen, *J. Am. Chem. Soc.* **129**, 960 (2007).

88. Y.B. Zheng, Y.W. Yang, L. Jensen, L. Fang, B.K. Juluri, A.H. Flood, P.S. Weiss, J.F. Stoddart, T.J. Huang, *Nano Lett.* **9**, 819 (2009).

89. A. Altieri, G. Bottari, F. Dehez, D.A. Leigh, J.K.Y. Wong, F. Zerbetto, *Angew. Chem. Int. Ed.* **42**, 2296 (2003).

90. P.R. Ashton, R. Ballardini, V. Balzani, A. Credi, K.R. Dress, E. Ishow, C.J. Kleverlaan, O. Kocian, J.A. Preece, N. Spencer, J.F. Stoddart, M. Venturi, S. Wenger, *Chem. Eur. J.* **6**, 3558 (2000).

91. F.G. Gatti, S. Lent, J.K.Y. Wong, G. Bottari, A. Altieri, M.A.F. Morales, S.J. Teat, C. Frochot, D.A. Leigh, A.M. Brouwer, F. Zerbetto, *Proc. Nat. Acad. Sci. U.S.A.* **100**, 10 (2003).

92. A.M. Brouwer, C. Frochot, F.G. Gatti, D.A. Leigh, L. Mottier, F. Paolucci, S. Roffia, G.W.H. Wurpel, *Science* **291**, 2124 (2001).

93. T.J. Huang, B. Brough, C.M. Ho, Y. Liu, A.H. Flood, P.A. Bonvallet, H.R. Tseng, J.F. Stoddart, M. Baller, S. Magonov, *Appl. Phys. Lett.* **85**, 5391 (2004).

94. Y. Liu, A.H. Flood, P.A. Bonvallett, S.A. Vignon, B.H. Northrop, H.R. Tseng, J.O. Jeppesen, T.J. Huang, B. Brough, M. Baller, S. Magonov, S.D. Solares, W.A. Goddard, C.M. Ho, J.F. Stoddart, *J. Am. Chem. Soc.* **127**, 9745 (2005).

95. B.K. Juluri, A.S. Kumar, Y. Liu, T. Ye, Y.W. Yang, A.H. Flood, L. Fang, J.F. Stoddart, P.S. Weiss, T.J. Huang, *ACS Nano* **3**, 291 (2009).

96. P.R. Ashton, I.W. Parsons, F.M. Raymo, J.F. Stoddart, A.J.P. White, D.J. Williams, R. Wolf, *Angew. Chem. Int. Ed.* **37**, 1913 (1998).

97. J.S. Wu, K.C.F. Leung, D. Benitez, J.Y. Han, S.J. Cantrill, L. Fang, J.F. Stoddart, *Angew. Chem. Int. Ed.* **47**, 7470 (2008).

98. J.W. Choi, A.H. Flood, D.W. Steuerman, S. Nygaard, A.B. Braunschweig, N.N.P. Moonen, B.W. Laursen, Y. Luo, E. DeIonno, A.J. Peters, J.O. Jeppesen, K. Xu, J.F. Stoddart, J.R. Heath, *Chem. Eur. J.* **12**, 261 (2006).

99. T.J. Huang, A.H. Flood, B. Brough, Y. Liu, P.A. Bonvallet, S.S. Kang, C.W. Chu, T.F. Guo, W.X. Lu, Y. Yang, J.F. Stoddart, C.M. Ho, *IEEE Trans. Autom. Sci. Eng.* **3**, 254 (2006).

100. W.Y. Zhang, W.R. Dichtel, A.Z. Stieg, D. Ben'tez, J.K. Gimzewski, J.R. Heath, J.F. Stoddart, *Proc. Nat. Acad. Sci. U.S.A.* **105**, 6514 (2008).

101. P. Kim, C.M. Lieber, *Science* **286**, 2148 (1999).

102. T. Rueckes, K. Kim, E. Joselevich, G.Y. Tseng, C.L. Cheung, C.M. Lieber, *Science* **289**, 94 (2000).

103. V.V. Deshpande, H.Y. Chiu, H.W.C. Postma, C. Miko, L. Forro, M. Bockrath, *Nano Lett.* **6**, 1092 (2006).

104. R.H. Baughman, C.X. Cui, A.A. Zakhidov, Z. Iqbal, J.N. Barisci, G.M. Spinks, G.G. Wallace, A. Mazzoldi, D. De Rossi, A.G. Rinzler, O. Jaschinski, S. Roth, M. Kertesz, *Science* **284**, 1340 (1999).

105. U. Vohrer, I. Kolaric, M.H. Haque, S. Roth, U. Detlaff-Weglikowska, *Carbon* **42**, 1159 (2004).

106. S. Gupta, M. Hughes, A.H. Windle, J. Robertson, *J. Appl. Phys.* **95**, 2038 (2004).

107. J.D.W. Madden, J.N. Barisci, P.A. Anquetil, G.M. Spinks, G.G. Wallace, R.H. Baughman, I.W. Hunter, *Adv. Mater.* **18**, 870 (2006).

108. T. Mirfakhrai, J. Oh, M. Kozlov, E.C.W. Fok, M. Zhang, S. Fang, R.H. Baughman, J.D.W. Madden, *Smart Mater. Struct.* **16**, S243 (2007).

109. Y. Yun, V. Shanov, Y. Tu, M.J. Schulz, S. Yarmolenko, S. Neralla, J. Sankar, S. Subramaniam, *Nano Lett.* **6**, 689 (2006).

110. L.T. Qu, Q. Peng, L.M. Dai, G.M. Spinks, G.G. Wallace, R.H. Baughman, *MRS Bull.* **33**, 215 (2008).

111. T. Mirfakhrai, J.D.W. Madden, R.H. Baughman, *Mater. Today* **10**, 30 (2007).

112. V.H. Ebron, Z.W. Yang, D.J. Seyer, M.E. Kozlov, J.Y. Oh, H. Xie, J. Razal, L.J. Hall, J.P. Ferraris, A.G. MacDiarmid, R.H. Baughman, *Science* **311**, 1580 (2006).

113. J.D. Madden, *Science* **318**, 1094 (2007).

114. G.M. Spinks, G.G. Wallace, L.S. Fifield, L.R. Dalton, A. Mazzoldi, D. De Rossi, I.I. Khayrullin, R.H. Baughman, *Adv. Mater.* **14**, 1728 (2002).

115. S.V. Ahir, E.M. Terentjev, *Nat. Mater.* **4**, 491 (2005).

116. H. Koerner, G. Price, N.A. Pearce, M. Alexander, R.A. Vaia, *Nat. Mater.* **3**, 115 (2004).

117. P. Miaudet, A. Derre, M. Maugey, C. Zakri, P.M. Piccione, R. Inoubli, P. Poulin, *Science* **318**, 1294 (2007).

118. S. Courty, J. Mine, A.R. Tajbakhsh, E.M. Terentjev, *Europhys. Lett.* **64**, 654 (2003).

119. S.G. Louie, *Top. Appl. Phys.* **80**, 113 (2001).

120. B. Vigolo, A. Penicaud, C. Coulon, C. Sauder, R. Pailler, C. Journet, P. Bernier, P. Poulin, *Science* **290**, 1331 (2000).

121. M. Zhang, K.R. Atkinson, R.H. Baughman, *Science* **306**, 1358 (2004).

122. M. Zhang, S.L. Fang, A.A. Zakhidov, S.B. Lee, A.E. Aliev, C.D. Williams, K.R. Atkinson, R.H. Baughman, *Science* **309**, 1215 (2005).
123. Y.L. Li, I.A. Kinloch, A.H. Windle, *Science* **304**, 276 (2004).
124. A.B. Dalton, S. Collins, E. Munoz, J.M. Razal, V.H. Ebron, J.P. Ferraris, J.N. Coleman, B.G. Kim, R.H. Baughman, *Nature* **423**, 703 (2003).
125. L.M. Ericson, H. Fan, H.Q. Peng, V.A. Davis, W. Zhou, J. Sulpizio, Y.H. Wang, R. Booker, J. Vavro, C. Guthy, A.N.G. Parra-Vasquez, M.J. Kim, S. Ramesh, R.K. Saini, C. Kittrell, G. Lavin, H. Schmidt, W.W. Adams, W.E. Billups, M. Pasquali, W.F. Hwang, R.H. Hauge, J.E. Fischer, R.E. Smalley, *Science* **305**, 1447 (2004).
126. R.H. Baughman, A.A. Zakhidov, W.A. de Heer, *Science* **297**, 787 (2002).
127. R.H. Baughman, *Synth. Met*. **78**, 339 (1996).
128. R.H. Baughman, L.W. Shacklette, R.L. Eisenbaumer, E.J. Plichta, C. Becht in *Conjugated Polymeric Materials: Opportunities in Electronics, Optoelectronics, and Molecular Electronics*. J.L. Brédas, R.R. Chance, Eds. (Kluwer, Dordrecht, 1990), pp. 559–582.
129. J.D.W. Madden, N.A. Vandesteeg, P.A. Anquetil, P.G.A. Madden, A. Takshi, R.Z. Pytel, S.R. Lafontaine, P.A. Wieringa, I.W. Hunter, *IEEE J. Oceanic Eng*. **29**, 706 (2004).
130. A.E. Aliev, J. Oh, M.E. Kozlov, A.A. Kuznetsov, S. Fang, A.F. Fonseca, R. Ovalle, M.D. Lima, M.H. Haque, Y.N. Gartstein, M. Zhang, A.A. Zakhidov, R.H. Baughman, *Science* **323**, 1575 (2009).
131. G.Y. Sun, J. Kurti, M. Kertesz, R.H. Baughman, *J. Phys. Chem. B* **107**, 6924 (2003).
132. Y.N. Gartstein, A.A. Zakhidov, R.H. Baughman, *Phys. Rev. B* **68** (2003). ☐